Photothermal nonlinearity and optical bistability in a graphene–silicon waveguide resonator

Cameron Horvath,[1,*] Daniel Bachman,[1] Rob Indoe,[2] and Vien Van[1]

[1]*Department of Electrical and Computer Engineering, University of Alberta, Edmonton, Alberta T6G 2V4, Canada*

[2]*National Institute for Nanotechnology, 11421 Saskatchewan Drive, Edmonton, Alberta T6G 2M9, Canada*

**Corresponding author: cshorvat@ualberta.ca*

Received September 9, 2013; accepted October 15, 2013;
posted October 28, 2013 (Doc. ID 197377); published November 22, 2013

We report observation of optical bistability and enhanced thermal nonlinearity in a graphene–silicon waveguide resonator. Photo-induced Joule heating in the graphene layer gives rise to a temperature increase in the silicon waveguide core and a corresponding thermo-optic shift in the resonance of the Fabry–Perot resonator. Measurement of the nonlinear resonance spectra showed a 9-fold increase in the effective thermal nonlinear index due to the graphene layer compared with a bare silicon waveguide.

OCIS codes: (130.2790) Guided waves; (190.4360) Nonlinear optics, devices; (190.1450) Bistability; (190.4870) Photothermal effects.

http://dx.doi.org/10.1364/OL.38.005036

Graphene has attracted significant attention from the photonics community due to its unique and useful optical properties, such as the ability to tune its optical absorption. Integrated photonic devices incorporating graphene in the waveguiding medium, such as polarizers, modulators, and couplers [1,2] have been demonstrated. However, interband absorption in the graphene waveguides [1–3] can cause a large amount of ohmic self-heating when excited with infrared or visible light. These thermal effects can be detrimental to the performance of some devices, but can also be used to realize efficient nonlinear thermo-optic devices such as switches [4]. Self-heating has been observed in a graphene-on-silicon waveguide [5], but to date there has been no reported study of photo-induced thermal nonlinearity in graphene waveguides.

In this Letter, we examine the propagation of light in a graphene–silicon waveguide resonator and investigate self-heating in the waveguide due to the graphene layer by experimentally measuring the photothermal resonance shift and optical bistability characteristics of the device. Numerical simulations of the temperature distribution in the waveguide are also performed and compared with the experimental results. We found that the graphene layer causes a 9-fold increase in the effective thermal nonlinear index for TM-polarized light compared with a bare silicon waveguide.

Silicon waveguides with a width of 2 μm and thickness of 340 nm were fabricated on a silicon-on-insulator (SOI) chip with a buried oxide thickness of 1 μm. The waveguides were patterned using electron-beam lithography and ICP reactive ion etching. The chip was then cleaved to provide smooth end facets that act as both the input/output ports of the device and reflectors for the Fabry–Perot resonator. The length of the waveguide resonator after cleaving was 3.3 mm.

Graphene was synthesized on copper foil with the chemical vapor deposition (CVD) method using methane in an Ar and H_2 environment at atmospheric pressure. After the foil was cooled, polymethyl-methacrylate (PMMA) was spun approximately 1 μm-thick onto the surface of the graphene and the foil was removed using an ammonium persulfate etchant. The remaining PMMA/graphene film was trimmed to a width of 2.5 mm and mechanically transferred onto the silicon waveguide, such that the graphene layer had direct contact with the top of the waveguide. To promote adhesion, the device was baked at 180°C (above the glass transition temperature of PMMA) for 45 min. The PMMA layer was kept on the device for mechanical support of the graphene layer. An optical micrograph of the graphene–silicon waveguide along with a schematic of the waveguide cross section are shown in Figs. 1(a) and 1(b). A Raman spectrograph of graphene produced using the CVD process is shown in Fig. 1(c). The positions and relative intensities of the G and $2D$ peaks indicate that bilayer graphene is mostly present [6]. The large D peak in the spectrum indicates that there are defects in the lattice of the graphene that will reduce

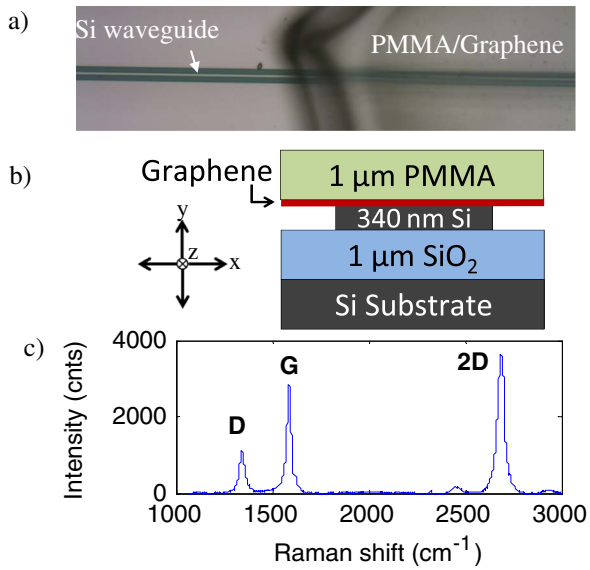

Fig. 1. (a) Optical micrograph of a graphene–Si waveguide with region of PMMA/graphene to the right. (b) Schematic of the graphene–Si waveguide. (c) Raman spectrograph of graphene fabricated with the CVD process.

the electrical conductivity [7] and optical absorbance of the graphene.

The spectral response of the waveguide resonator was measured using a CW tunable laser and lensed fibers that were butt-coupled to the input/output facets of the waveguide. The coupling loss was measured to be 13.5 dB/facet for TM polarization and 14.7 dB/facet for TE. The spectral response of the silicon waveguide resonator without PMMA/graphene is shown in Fig. 2, and was measured using a low input power of 500 μW. The reflectance of $R = 0.35$ per waveguide facet and free spectral ranges (FSR) of 85.1 pm and 102.3 pm were found from the resonance spectrums for TM and TE polarization, respectively. From the FSR, the group index was found to be 4.28 for TM polarization and 3.56 for TE. After the PMMA/graphene layer was transferred onto the waveguide, the propagation loss increased to 19.3 dB/cm for TM polarization and 9.8 dB/cm for TE. These loss values are slightly lower in magnitude to the graphene waveguide losses reported in [1], where a polymer core was used instead of silicon. The propagation loss is attributed mainly to the optical absorbance of the graphene layer. Simulations of the graphene–Si waveguide modes showed that, to match the measured propagation loss values, the electrical conductivity σ of the graphene layer had to be reduced by about an order of magnitude below the theoretical value of $\sigma_{2D} = e^2/4\hbar$ [8]. The reduced conductivity may be caused by lattice defects in our graphene layer as evidenced by the large D peak in the Raman spectrum of Fig. 1(c).

The light absorbed in the graphene layer is converted to heat, which causes a change in the effective index of the waveguide due to the thermo-optic effect in the silicon core. This change in the effective index manifests itself as a shift in the resonance spectrum of the waveguide resonator. Figures 3(a) and 3(b) show the measured spectral responses of the device at various input power levels for TE and TM polarizations. The input power is defined here as the net power (after butt coupling loss is subtracted) that is coupled into the waveguide resonator. As the input power is increased, we observe a redshift in the resonant wavelength and the resonance spectra become increasingly asymmetric with a steepened transition edge, which is indicative of optical bistability. In Fig. 3(c) we plotted the peak resonant wavelength shift versus input power for both polarizations in the graphene–Si waveguide. For comparison, we also plotted the resonance shift in the bare Si waveguide for the TM mode. In all three cases, the resonance shift is positive and varies linearly with the input power. With the addition of the graphene layer,

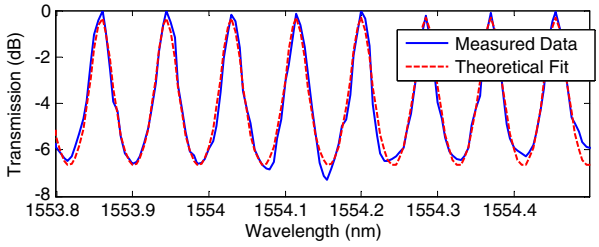

Fig. 2. Spectral response of the Si waveguide resonator without graphene for TM polarization.

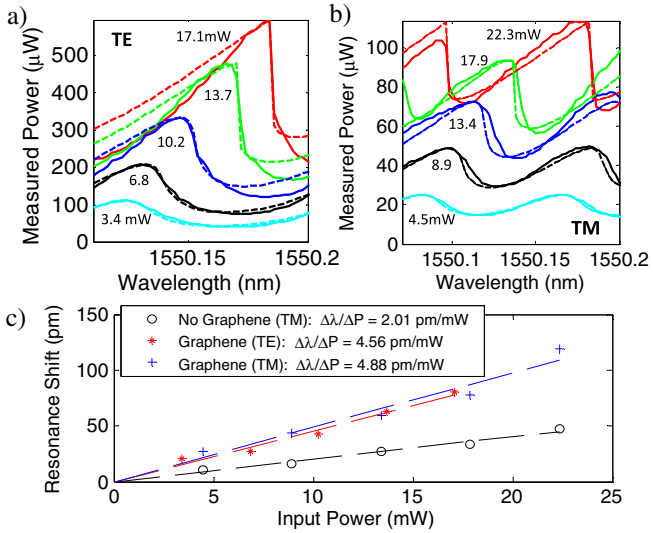

Fig. 3. Spectral responses of the graphene–Si waveguide resonator at varying input powers for (a) TE mode, (b) TM mode (solid lines are measurements, dashed lines are theoretical fits). (c) Dependence of the resonant wavelength shift on the input power.

the TE mode exhibits resonance shift at a rate of $\Delta\lambda/\Delta P_{\text{in}} = 4.56$ pm/mW, which is comparable with that of the TM mode, $\Delta\lambda/\Delta P_{\text{in}} = 4.88$ pm/mW. Both of these values are larger than the rate of resonance shift exhibited in the bare silicon waveguide, $\Delta\lambda/\Delta P_{\text{in}} = 2.01$ pm/mW, indicating that the photothermal effect is more pronounced in the graphene–Si waveguide. Defining the effective thermal nonlinear index n_2 for the waveguide as $\Delta n = n_2 I$, where I is the intensity, we obtained $n_2 = 1.8 \times 10^{-10}$ cm^2/W for TM and 5.6×10^{-11} cm^2/W for TE in the graphene–Si waveguide. The larger n_2 value for TM polarization arises mainly because of the larger magnitude of the tangential electric field in the graphene layer for the TM mode, which causes more ohmic heating. The effective area of the TM mode (0.760 μm^2) is also larger than the area of the TE mode (0.490 μm^2), which reduces the intensity for the same power. The thermal nonlinear index obtained for the TM mode in the bare Si waveguide is $n_2 = 2.0 \times 10^{-11}$ cm^2/W, which is 9 times lower than when the graphene layer was present. These measurements also confirm that the observed nonlinearity is predominantly thermal in origin, since free-carrier dispersion would result in a blueshift of the resonant wavelength and Kerr nonlinearity (reported in [3] for a similar graphene–Si waveguide) is two orders of magnitude lower than the n_2 values obtained here.

To theoretically investigate the self-heating effect in the graphene–silicon waveguide, we performed numerical simulations to determine the electric field and steady-state temperature distributions in the waveguide using the COMSOL finite element software. In the simulations, graphene was modeled as a thin film with a bulk electrical conductivity of $\sigma_{3D} = \sigma_{2D}/\Delta$ [2], where $\Delta = 0.7$ nm is the effective thickness of the graphene layer and $\sigma_{2D} = 3.5 \times 10^{-6}\ \Omega^{-1}$, as determined from the measured propagation loss in the waveguide resonator. Figures 4(a)–4(d) show the TE and TM modal

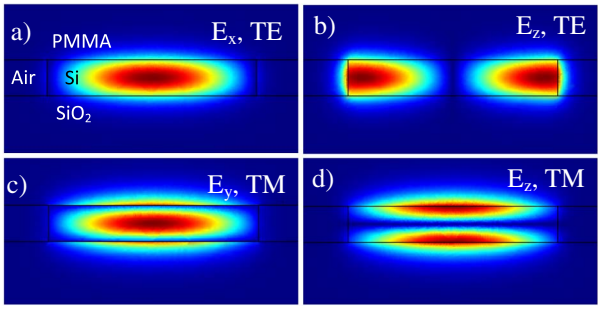

Fig. 4. Modal electric field distributions in the graphene–Si waveguide: (a) E_x, (b) E_z for TE polarization, (c) E_y, and (d) E_z for TM polarization.

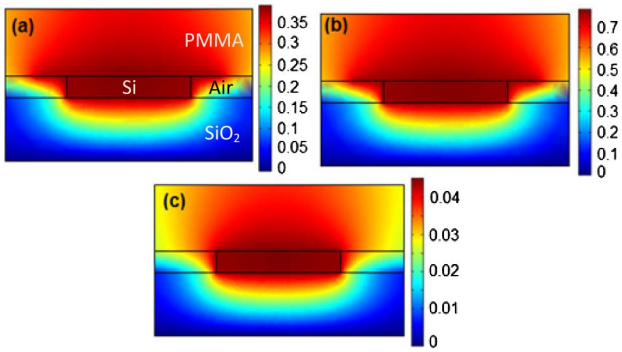

Fig. 5. Steady-state temperature distribution (relative to 295 K) at 5 mW input power for (a) TE mode, (b) TM mode in the graphene–Si waveguide, and (c) TM mode in bare Si waveguide without PMMA/graphene.

distributions of the electric field components. Note that the field components that are in the plane of the graphene layer will contribute predominantly to ohmic heating in the graphene sheet.

The steady-state temperature distribution T in the waveguide was then obtained by solving the heat equation:

$$-\nabla \cdot (K\nabla T) = q, \tag{1}$$

where K is the thermal conductivity and q is the heat source resulting from the absorption of light. The thermal conductivity values used were 149, 1.4, 0.25, and 5000 $\mathrm{W/m \cdot K}$ [9] for Si, SiO_2, PMMA, and graphene, respectively. The heat source is calculated from the modal electric field distribution using:

$$q = \frac{1}{2}\sigma|\vec{E}|^2, \tag{2}$$

where σ is the electrical conductivity of the material. The electrical conductivity for silicon is computed from its absorption coefficient ($\alpha = 1$ dB/cm [10]) using:

$$\sigma = \alpha n\sqrt{\varepsilon_0/\mu_0}, \tag{3}$$

where n is the index of refraction. The absorption is assumed to be negligible in the PMMA and SiO_2 layers. Figures 5(a)–5(c) show the temperature distributions at 5 mW input power for the TE and TM modes in the graphene–Si waveguide, and for the TM mode in the bare Si waveguide. Ohmic heating in the graphene layer and dielectric heating in the silicon core both contribute to the temperature rise, although the former is dominant. The values of the temperature and corresponding nonlinear index are listed in Table 1. It is seen that the calculated n_2 values are in close agreement with the measured values for both TE and TM modes of the graphene–Si waveguide as well as for the TM mode of the bare Si waveguide.

The measured resonant spectra in Figs. 3(a) and 3(b) were fitted using the optical dispersive bistability model for a Fabry–Perot resonator described in [11] and the results are shown by the dashed lines in the plots. From the bistability curves, we obtained $n_2 = 1.8 \times 10^{-10}$ $\mathrm{cm^2/W}$ for TM and 5.4×10^{-11} $\mathrm{cm^2/W}$ for TE. The input power threshold for the onset of bistability was found to be 11.0 mW for TE and 14.1 mW for TM in the graphene–Si resonator. The value for the TM mode is larger than the value of 11.8 mW obtained for the TM mode in the bare Si waveguide resonator even though the graphene–Si waveguide has stronger thermal nonlinearity. This is because the graphene layer also induces larger attenuation in the waveguide, thus, requiring higher input power to reach optical bistability in the graphene–Si resonator. The steady-state input versus output power transfer function for the graphene–Si waveguide resonator is shown in Fig. 6 for TM polarization at 1550.138 nm wavelength. The hysteresis indicates bistability where two stable output powers can be obtained for a given input power. The measured data corresponds to the direction of increasing power on the hysteresis loop.

In summary, we reported enhanced photothermal nonlinear effects due to the addition of a graphene layer on a silicon waveguide and measured the effective thermal nonlinear indices for both polarizations. In general, the thermal nonlinear index is dependent on the quality of the graphene layer via its optical absorbance, as well as the geometry of the waveguide structure. For example, in some graphene–Si waveguides [12], the graphene layer is separated from the Si core by a thin HSQ layer, which leads to lower waveguide loss and, hence, less self-heating. The PMMA cladding layer also has the effect of lowering the thermal nonlinear index, since PMMA has a

Table 1. Simulation and Experimental Results for the Effective Thermal Nonlinear Index n_2

Structure	Temperature ΔT (K) (Simulation)	Effective Nonlinear Index n_2 ($\mathrm{cm^2/W}$) (Simulation)	Effective Nonlinear Index n_2 ($\mathrm{cm^2/W}$) (Experimental)
Graphene–Si (TE)	0.39	7.1×10^{-11}	5.6×10^{-11}
Graphene–Si (TM)	0.74	2.1×10^{-10}	1.8×10^{-10}
Bare Si (TM)	0.045	1.3×10^{-11}	2.0×10^{-11}

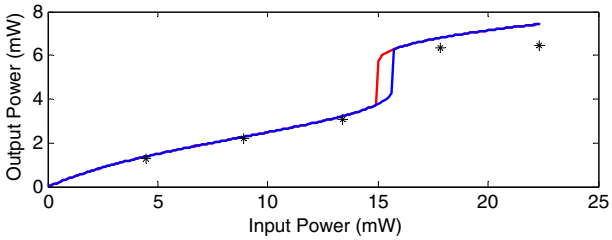

Fig. 6. Steady-state transfer function of the graphene–Si waveguide resonator for TM polarization at 1550.138 nm (starred points are measurements; lines are obtained from the dispersive bistability model using experimentally measured thermal nonlinear index n_2).

negative thermo-optic coefficient (-1.2×10^{-4} K^{-1} [13]), which slightly counteracts the positive index shift in the Si core. Therefore, we expect to see stronger photothermal nonlinearity if the PMMA layer is removed, as is the case for some graphene–Si structures [3]. The observed optical bistability is also expected to be more pronounced in high quality factor resonators, such as micro-rings and photonic crystal cavities, making them potentially useful as thermo-optic switches. Finally we note that graphene has one of the largest thermal conductivities of any material, and this may help to reduce the thermal response time of these devices by rapidly spreading heat away from the waveguide core.

This work was supported by the Natural Sciences and Engineering Research Council of Canada (NSERC).

References

1. J. T. Kim and C. G. Choi, Opt. Express **20**, 3556 (2012).
2. A. Locatelli, A. Capobianco, M. Midrio, S. Boscolo, and C. De Angelis, Opt. Express **20**, 28479 (2012).
3. T. Gu, N. Petrone, J. F. McMillan, A. van der Zande, M. Yu, G. Q. Lo, D. L. Kwong, J. Hone, and C. W. Wong, Nat. Photonics **6**, 554 (2012).
4. D. Perron, M. Wu, C. Horvath, D. Bachman, and V. Van, Opt. Lett. **36**, 2731 (2011).
5. Z. Cheng, H. K. Tsang, X. Wang, K. Xu, and J. B. Xu, IEEE J. Sel. Topics Quantum Electron. **20**, 1 (2014).
6. Z. Yan, Z. Peng, Z. Sun, J. Yao, Y. Zhu, Z. Liu, P. M. Ajayan, and J. M. Tour, ACS Nano **5**, 8187 (2011).
7. J. Kang, D. Shin, S. Bae, and B. H. Hong, Nanoscale **4**, 5527 (2012).
8. L. A. Falkovsky, J. Phys. Conf. Ser. **129**, 012004 (2008).
9. A. A. Balandin, S. Ghosh, W. Bao, I. Calizo, D. Teweldebrhan, F. Miao, and C. N. Lau, Nano Lett. **8**, 902 (2008).
10. A. Grieco, B. Slutsky, D. T. H. Tan, S. Zamek, M. P. Nezhad, and Y. Fainman, J. Lightwave Technol. **30**, 2352 (2012).
11. R. W. Boyd, *Nonlinear Optics*, 3rd ed. (Academic, 2008), pp. 359–365.
12. H. Li, Y. Anugrah, S. J. Koester, and M. Li, Appl. Phys. Lett. **101**, 111110 (2012).
13. J. M. Cariou, J. Dugas, L. Martin, and P. Michel, Appl. Opt. **25**, 334 (1986).